Band structure of absorptive two-dimensional photonic crystals

Han van der Lem and Adriaan Tip

Fundamenteel Onderzoek der Materie, Instituut voor Atoom- en Molecuulfysica, Kruislaan 407, 1098SJ Amsterdam, The Netherlands

Alexander Moroz*

Debye Instituut, Universiteit Utrecht, P.O. Box 80000, 3508 TA Utrecht, The Netherlands

Received September 12, 2002; revised manuscript received January 14, 2003

The band structure for an absorptive two-dimensional photonic crystal made from cylinders consisting of a Drude material is calculated. Absorption causes the spectrum to become complex and form islands in the negative complex half-plane. The boundaries of these islands are not always formed by the eigenvalues calculated for Bloch vectors on the characteristic path, and we find a hole in the spectrum. For realistic parameter values, the real part of the spectrum is hardly influenced by absorption, typically less than 0.25%. The employed method uses a Korringa–Kohn–Rostoker procedure together with analytical continuation. This results in an efficient approach that allows these band-structure calculations to be done on a Pentium III personal computer.

OCIS codes: 290.4210, 260.2110, 240.6680, 260.3910.

1. INTRODUCTION

Photonic crystals (PCs) are dielectric structures with an electric permeability (dielectric function, permittivity) $\varepsilon(\mathbf{x})$, possessing a spatial periodicity, i.e., $\varepsilon(\mathbf{x}) = \varepsilon(\mathbf{x} + \mathbf{a}_j)$. Depending on the number of independent lattice vectors $\mathbf{a}_j$, we are dealing with one-dimensional (1D), two-dimensional (2D), or three-dimensional (3D) photonic crystals. They offer new ways of manipulating the emission and propagation of light. The propagation of radiation inside a PC is affected by the periodicity in a way similar to that of an electron traveling in a periodic potential in an ordinary (semiconductor) crystal, giving rise to the photonic analog of the well-known band structures of solid-state physics.[1–4] Depending on their properties, such as the lattice type and its constituting materials, PCs can exhibit complete photonic bandgaps (CPBGs), a frequency domain in which the propagation of radiation is inhibited, irrespective of direction and polarization. Also, partial or stop gaps can be present, in which case radiation cannot propagate in certain directions but can in others.

In order to obtain a CPBG, strong scattering is needed, and hence a large contrast of dielectric constants is required. In the optical region, only a limited number of dielectrics are available with a sufficiently high dielectric constant. However, recent calculations[5–8] showed that photonic crystals, made from metallic spheres, exhibiting a Drude-like behavior, in a dielectric background, can have large CPBGs. An example of such a metal is silver, in which case large CPBGs are found for 3D photonic crystals and, for propagation in the plane of periodicity, also for 2D photonic crystals. Here it was assumed that ε depends on both position and frequency, $\varepsilon = \varepsilon(\mathbf{x}, \omega)$, but is real, i.e., there is dispersion but absorption is absent.

Since absorption can be appreciable in certain frequency ranges, this raises the question as to what happens in such a situation. Two objects are of importance, the band structure and Green's functions. The first can give information about decay in time due to absorption and the second about the attenuation of a beam traveling through an absorptive PC. Moreover, the imaginary part of the Green's function also appears in expressions for the radiative decay of embedded atoms.[9]

In the absorptive case, Maxwell's equations are

$$\begin{aligned}
\partial_t \mathbf{D}(\mathbf{x}, t) &= \partial_{\mathbf{x}} \times \mathbf{B}(\mathbf{x}, t) - \mathbf{J}(\mathbf{x}, t),\\
\partial_t \mathbf{B}(\mathbf{x}, t) &= -\partial_{\mathbf{x}} \times \mathbf{E}(\mathbf{x}, t),\\
\partial_{\mathbf{x}} \cdot \mathbf{D}(\mathbf{x}, t) &= \rho(\mathbf{x}, t), \qquad \partial_{\mathbf{x}} \cdot \mathbf{B}(\mathbf{x}, t_0) = 0,\\
\mathbf{D}(\mathbf{x}, t) &= \varepsilon_0 \mathbf{E}(\mathbf{x}, t) + \mathbf{P}(\mathbf{x}, t),\\
\mathbf{P}(\mathbf{x}, t) &= \int_{-\infty}^{t} \mathrm{d}s\, \chi(\mathbf{x}, t - s)\mathbf{E}(\mathbf{x}, s),
\end{aligned} \tag{1}$$

where $\chi(\mathbf{x}, t)$ is the electric susceptibility. Substitution of a harmonic solution

$$\mathbf{u}(\mathbf{x}, \omega, t) = \exp[-i\omega t]\mathbf{u}(\mathbf{x}, \omega) \tag{2}$$

results in the Helmholtz equation (U is the unit 3×3 matrix and c, the speed of light, is set equal to 1, so $\varepsilon_0 = 1$),

$$[\omega^2 \varepsilon(\mathbf{x}, \omega) - \mathsf{H}_0]\mathbf{u}(\mathbf{x}, \omega) = 0, \qquad \mathsf{H}_0 = -\partial_{\mathbf{x}}^2 \mathsf{U} + \partial_{\mathbf{x}} \partial_{\mathbf{x}}, \tag{3}$$

featuring the space- and frequency-dependent, complex, electric permeability

$$\varepsilon(\mathbf{x}, \omega) = 1 + \hat{\chi}(\mathbf{x}, \omega),$$

0740-3224/2003/061334-08$15.00

$$\hat{\chi}(\mathbf{x},\ \omega) = \int_0^\infty \mathrm{d}t\ \exp[i\omega t]\chi(\mathbf{x},\ t). \tag{4}$$

From a fundamental point of view, the presence of absorption raises a number of questions. If we try to determine the field modes $\mathbf{u}(\mathbf{x}, \omega)$, it turns out that, in absorptive frequency regions ($\mathrm{Im}\,\varepsilon(\mathbf{x},\ \omega) \neq 0$), no solutions exist for real ω. This is not unexpected, absorption giving rise to decay and hence no purely oscillating behavior. We recall that the integrated density of states is obtained by counting eigenvalues, up to a certain value, for a system in a box, and then by taking a thermodynamic limit; means that this quantity is no longer defined. But then it is not obvious how bandgaps can be defined.

Recently, Tip *et al.*,[10] in a mathematical analysis of the problem, proposed a definition of bandgaps for this case. Thus if for any initial fields at time $t = t_0$, the Fourier transform $\tilde{\mathbf{E}}(\omega)$ of the electric field $\mathbf{E}(t)$ vanishes for ω in a certain range Δ, then Δ is said to be a bandgap. This means that field modes with frequency $\omega \in \Delta$ are absent, and this definition coincides with the usual one in the nonabsorptive case. The above authors then showed that such bandgaps Δ do not occur in absorptive frequency regions. This can be understood by realizing that bandgaps are connected to the vanishing of the coherent sum of reflected waves from an infinite number of scatterers on lattice positions. But if a wave is attenuated before and after being scattered from a particular scatterer, the total reflected wave is changed and need no longer vanish. In the above reference, it was also found, making a Bloch decomposition and using analytic continuation techniques, that, for a fixed vector $\mathbf{k}$ from the first Brillouin zone $\mathcal{B}$, the eigenvalues $\omega(\mathbf{k})$ (which are real and make up the bands as $\mathbf{k}$ runs through $\mathcal{B}$ in the nonabsorptive case) become complex (they turn into resonances) and give rise to areas in the negative complex half-plane. The basic requirement for this is that the complex dielectric function ($\chi(t)$ is the electric susceptibility)

$$\varepsilon(\omega) = 1 + \int_0^\infty \mathrm{d}t\ \exp[i\omega t]\chi(t), \tag{5}$$

which has an analytic continuation in the upper half-plane, can also be continued in the lower half-plane. Then we can find solutions of Eq. (3) with $\omega \to z$, $z \in \mathbb{C}_-$, the lower complex half-plane, but their meaning only becomes clear after the analysis in Ref. 10.

In this work we complement these findings with a numerical investigation for an absorptive 2D photonic crystal, consisting of Drude-like cylinders on a square lattice in a nonabsorptive host material with the dielectric constant ε_h. Thus the system shows nontrivial periodicity in two directions and is homogeneous in the third, with the lattice vectors' magnitudes taken of the order of an optical wavelength. The dielectric function of Drude-like materials reads

$$\varepsilon(\omega) = 1 - \frac{\omega_p^2}{\omega(\omega + i\gamma)}, \tag{6}$$

which has the correct analytic continuation properties for the above analysis to be applicable.

In earlier work,[8] we considered the silver case, using the experimental $\mathrm{Re}\,\varepsilon(\omega)$ and neglecting absorption, i.e., the system is dispersive but not absorptive. In the optical regime, silver has a large frequency window for which $\mathrm{Im}\,\varepsilon(\omega)$ remains approximately constant at a value of 0.5, which is very small as compared with the values of $\mathrm{Im}\,\varepsilon(\omega)$ in other metals. Outside this window, it rapidly takes on values of 10 and higher. Inside this low $\mathrm{Im}\,\varepsilon$ frequency window, we found a CPBG with a relative gap width (the gap width expressed as a percentage of the midgap frequency) of 9.9% for silver scatterers in an air host dielectric. $\mathrm{Re}\,\varepsilon(\omega)$ is negative in this frequency window, and we found that the size of the gap increases with increasing dielectric constant of the host material. In addition, we found a CPBG with a relative width of ~37% in a frequency range where the imaginary part of the dielectric constant is significantly above 0.5.

2. METHOD

We performed our band-structure calculations with a 2D photonic version of the Korringa–Kohn–Rostoker (KKR) method.[11,12] For the 3D case, see Ref. 13. It uses a Green's functions approach and has as basic building blocks the single particle (in our case cylinder) transition matrix on the energy shell and the so-called structure constants (see the appendix for the definition). This method has a number of significant advantages that make it quite suitable for the type of systems we are dealing with. We consider PCs with circular cylindrical scatterers. Up to now, most experimental work on 2D photonic crystals has dealt with such PCs. According to the KKR procedure, the fields are decomposed into a set of cylindrical harmonics. Thus we take advantage of the symmetry of the scatterers and achieve rapid convergence, in most cases with cylindrical harmonics with angular-momentum quantum number $m \leqslant 8$. Also, dispersion is no problem within the KKR method, which is obviously very important when dealing with dispersive media such as metals.

We have chosen the parameters of the Drude-model dielectric function such that it resembles the dielectric function of silver as closely as possible. For silver, the real part of the experimental $\varepsilon_{\mathrm{Ag}}(\omega)$ closely follows the Drude expression throughout a large frequency window, except for frequencies very close to the zero crossing ω_0 of $\mathrm{Re}\,\varepsilon(\omega)$, and we fitted ω_p to the experimental data of silver in this frequency window. Previously, where we neglected the absorption, we found the large CPBGs mentioned above by varying the lattice spacing a and filling fraction f. In order to see the influence of the presence of absorption on these results, we again have chosen the same values for these parameters: $\omega_p = 1.1(2\pi c/a)$ (numerical values of ω are identical to that of a/λ) and $f = 65\%$. In contrast with $\mathrm{Re}\,\varepsilon(\omega)$, $\mathrm{Im}\,\varepsilon(\omega)$ remains more or less constant at a value of 0.5 in a large frequency window in the visible. Since we want to verify the assumption that a realistic amount of absorption does not influence the previous results (see Ref. 14), we have taken γ such that $\mathrm{Im}\,\varepsilon_{\mathrm{Drude}}(\omega) \geqslant \mathrm{Im}\,\varepsilon_{\mathrm{Ag}}(\omega)$ in this frequency window of low $\mathrm{Im}\,\varepsilon_{\mathrm{Ag}}$, so we chose $\gamma = 0.05(2\pi c/a)$.

In the absence of absorption, the eigenvalues $\omega(\mathbf{k})$, which form the band structure, are all real. According to the KKR method, these eigenvalues are the roots of the determinant

$$D(\omega, \mathbf{k}) = \det[1 - t(\omega)g(\omega, \mathbf{k})], \tag{7}$$

i.e., the values of ω for which $D(\omega, \mathbf{k}) = 0$ for fixed $\mathbf{k}$, where t is the "on-the-energy-shell" single-scatterer transition matrix, and g is a matrix containing the structure constants (see also the appendix). As discussed above, these eigenvalues become complex in the presence of absorption, i.e., the real eigenvalues turn into resonances. In the following, we denote these complex eigenvalues as $z(\mathbf{k})$ in order to distinguish them from the real eigenvalues $\omega(\mathbf{k})$ of the nonabsorptive case. In the corresponding solution

$$\mathbf{u}(\mathbf{x}, z, t) = \exp[-iz(\mathbf{k})t]\mathbf{u}(\mathbf{x}, z) \tag{8}$$

of the Bloch-decomposed Helmholtz equation, $\mathrm{Im}\, z(\mathbf{k})$ is the decay rate of the eigenmode. The real spectrum of the nonabsorptive case is now replaced by the complex set

$$\mathcal{C} = \{z(\mathbf{k}) | \mathbf{k} \in \mathcal{B}\}, \tag{9}$$

in the lower complex half-plane.

Without absorption, $D(\omega, \mathbf{k})$ is a real function of the real argument ω. When we fix $\mathbf{k}$, we are left with the 1D problem of finding the real and nonnegative roots $\omega_j(\mathbf{k})$ on the real ω axis. One-dimensional root finding is very robust: If $D(\omega_1, \mathbf{k})$ and $D(\omega_2, \mathbf{k})$ have a different sign, there must be either a root or a pole in the interval (ω_1, ω_2). They are easily distinguished, and excellent algorithms exist for their determination.

With absorption included, the eigenvalues become complex, so $D(z, \mathbf{k})$ must be considered for complex z, and we have to use 2D root-finding algorithms for their determination. Most of the algorithms for finding a root in higher dimensions rely on having a sufficiently accurate initial guess of the location of the root. If the initial guess is not good enough, the root-finding algorithm might not find the root one is after. An obvious way of getting a proper initial guess is by initially neglecting the absorption. As said, robust 1D root finding can be employed to obtain the real eigenvalues $\omega(\mathbf{k})$. Since, as mentioned earlier, we assume that the band structures are not affected significantly by the presence of realistic amounts of absorption, we expect the actual complex eigenvalues $z(\mathbf{k})$ to be close to the real eigenvalues $\omega(\mathbf{k})$. Therefore it would seem likely that $\omega(\mathbf{k})$ is a good first guess to be used by the 2D root-finding routine to calculate $z(\mathbf{k})$.

In this paper, we only consider fields propagating in the plane of periodicity. In that case, the field equations can be decoupled into two scalar ones, one for each polarization. By E polarization, we mean the polarization for which the $\mathbf{E}$ field is parallel to the symmetry axis, and for the H polarization the $\mathbf{H}$ field is parallel to the symmetry axis.

A. *E* Polarization

For the E polarization, we applied the above strategy of first calculating $\omega(\mathbf{k})$ and use this as a first estimate to be used for the 2D root-finding routine in order to calculate $z(\mathbf{k})$.

B. *H* Polarization

For the H polarization, this strategy had to be refined. Previously, we found a large number of flat bands in the frequency domain centered around $\omega_{\mathrm{sp}} = \omega_p/(1 + \varepsilon_{\mathrm{h}})^{1/2}$, the surface-plasmon frequency for a flat interface. In the vicinity of these flat bands, $D(z, \mathbf{k})$ behaves very wildly since its roots and poles are lying very close to each other. Under these conditions, the root-finding routine we employed for the E polarization was not able to produce $z(\mathbf{k})$ if $\omega(\mathbf{k})$ was used as an initial estimate. We obtained an improved estimate for the position of a complex eigenvalue by exploiting the fact that $D(z, \mathbf{k})$ is analytic outside its poles. Then, by Cauchy's formula, denoting by $\mathrm{Res}(D^{-1}; z_0)$, the residue in the pole z_0 of $D^{-1}(z, \mathbf{k})$ and Γ a contour around z_0, avoiding other poles of $D^{-1}(z, \mathbf{k})$:

$$\oint_\Gamma D^{-1}(z, \mathbf{k})dz = 2\pi i\ \mathrm{Res}(D^{-1}; z_0), \tag{10}$$

$$\oint_\Gamma zD^{-1}(z, \mathbf{k})dz = 2\pi i\ \mathrm{Res}((zD^{-1}); z_0) = 2\pi i z_0\ \mathrm{Res}(D^{-1}; z_0). \tag{11}$$

This procedure has the advantage that poles of $D(z, \mathbf{k})$ appear as zeros of $D^{-1}(z, \mathbf{k})$ and are harmless in the contour integration. This leads to a satisfactory estimate of z_0 from the ratio of Eqs. (10) and (11). Thus we first calculated the real eigenvalue with absorption neglected. Next, we estimated from this eigenvalue the area in the complex plane where the root of $D(z, \mathbf{k})$ is expected to appear. We then evaluated $D(z, \mathbf{k})$ for 20 values of z on a square contour enclosing this area, and from this we obtained an approximation of both integrals. This procedure rendered an excellent starting value, which, upon insertion into the original 2D root-finding routine, quickly converged to the complex root, typically within six iterations.

It is not necessary to go through the whole process described above for every Bloch vector $\mathbf{k}$. Indeed, once the spectrum has been calculated for two close $\mathbf{k}$ values, we can simply extrapolate the eigenvalues associated with the two previous Bloch vectors to obtain an excellent initial estimate. As a result, once the complex eigenvalues are calculated for two $\mathbf{k}$ vectors, calculating the rest of $\mathcal{C}$ requires only minor computational effort and is calculated very fast. Although we did not do so, this procedure also opens the way to obtain the $z(\mathbf{k})$ values for larger values of $\mathrm{Im}\, \varepsilon$. Once a $z(\mathbf{k})$ is found for certain $\mathrm{Im}\, \varepsilon$, we can use it as an input for finding $z(\mathbf{k})$ for a slightly larger $\mathrm{Im}\, \varepsilon$ and so on.

3. RESULTS

In Figs. 1 and 2, we present some of our results for the E and H polarizations, respectively. The lower parts of these figures show the eigenvalues $z_j(\mathbf{k})$ in the complex

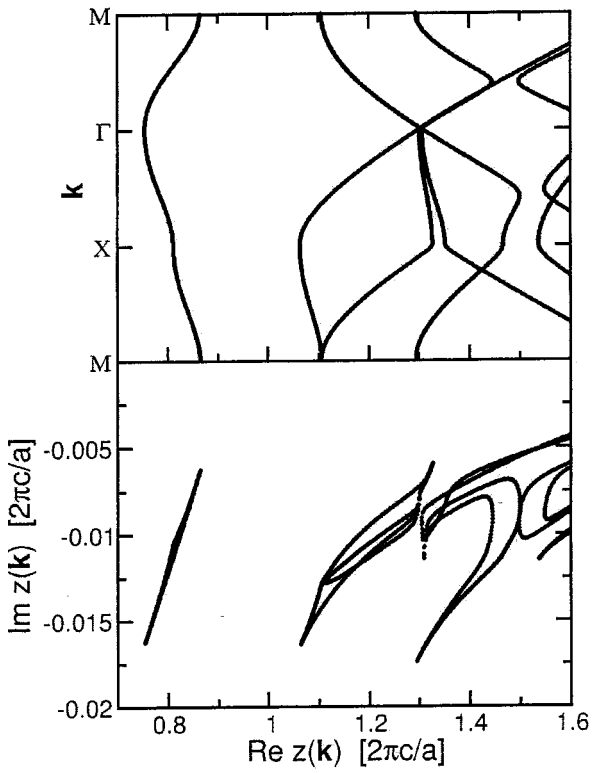

Fig. 1. Complex eigenvalues and the real part of the band structure calculated on the characteristic path for the E polarization. The lower graph shows the eigenvalues in the complex plane. The upper graph shows the real part of the band structure.

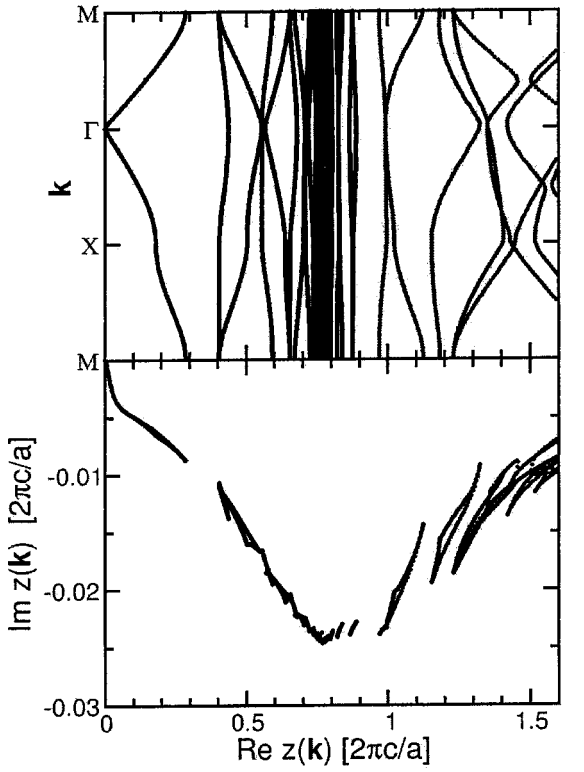

Fig. 2. Complex eigenvalues and the real part of the band structure calculated on the characteristic path for the H polarization. The lower graph shows the eigenvalues in the complex plane. The upper graph shows the real part of the band structure.

plane (fourth quadrant) calculated for Bloch vectors $\mathbf{k}$ on the so-called characteristic path $\mathcal{B}_c$ (connecting the special points of high symmetry in the Brillouin zone). For comparison with nonabsorptive photonic band plots $\{\omega_j(\mathbf{k})|\mathbf{k} \in \mathcal{B}_c\}$, we also plot $\mathrm{Re}\, z_j(\mathbf{k})$ as $\mathbf{k}$ runs through $\mathcal{B}_c$, in the upper part of Figs. 1 and 2. Below, we refer to $\{z_j(\mathbf{k})|\mathbf{k} \in \mathcal{B}_c\}$ as the jth (complex) band, and $\{\mathrm{Re}\, z_j(\mathbf{k})|\mathbf{k} \in \mathcal{B}_c\}$ as the real part of the jth (complex) band. Without absorption, this definition coincides with the ordinary definition of bands. To make a comparison between the real bands $\{\omega_j(\mathbf{k})|\mathbf{k} \in \mathcal{B}_c\}$ and the real parts of the complex bands $\{\mathrm{Re}\, z_j(\mathbf{k})|\mathbf{k} \in \mathcal{B}_c\}$ more transparent, we exchanged the plot axes of the upper plots so that the horizontal axes of both the upper and the lower plots are the same. Bands can, but need not, overlap, and their union constitutes the spectrum, which may or may not cover the nonnegative real axis. In the real case, the breaks in the spectrum are the band gaps.

With absorption included, the eigenvalues acquire a negative imaginary part. The bands on the characteristic path of the nonabsorptive case now change into closed loops $\{z_j(\mathbf{k})|\mathbf{k} \in \mathcal{B}_c\}$ in the fourth quadrant of the complex plane. If we increase the Drude model parameter γ, thereby increasing the $\mathrm{Im}\, \varepsilon(\omega)$ for all ω, $|\mathrm{Im}\, z_j(\mathbf{k})|$ increases monotonically, for all j and $\mathbf{k}$.

From the lower plots in Figs. 1 and 2, we see that, even within the same band $\{z_j(\mathbf{k})|\mathbf{k} \in \mathcal{B}_c\}$, the decay rate $\mathrm{Im}\, z_j(\mathbf{k})$ can vary significantly. For instance, for the band of the E polarization lowest in frequency at $\mathrm{Re}\, z(\mathbf{k}) \approx 0.8$, the ratio $\mathrm{Im}\, z(\mathbf{k}_M)/\mathrm{Im}\, z(\mathbf{k}_\Gamma)$ of the decay rates at the M point and at the Γ point has a value of 2.75. This ratio is very sensitive to the value of the filling fraction. It increases if we lower the filling fraction. For instance, at a filling fraction of 30%, $\mathrm{Im}\, z(\mathbf{k}_M)/\mathrm{Im}\, z(\mathbf{k}_\Gamma)$ already reaches a value of 10, and it increases further for a decreasing filling fraction. Below this band, there are no more bands, as was already known from the absorptionless calculations.

The results for the H polarization are shown in Fig. 2. In the upper part, we see the well-known[8,14] real part of the band structure consisting of both dispersive bands and a high number of very flat bands centered around the surface-plasmon frequency $\omega_{\mathrm{sp}} = \omega_p/\sqrt{2}$. We see that these flat bands have the highest decay rates $|\mathrm{Im}\, z(\mathbf{k})|$ and are quite insensitive to the value of $\mathbf{k}$. Upon decreasing the frequency ($\mathrm{Re}\, z$) below ω_{sp}, $|\mathrm{Im}\, z|$ decreases again until it reaches $\mathrm{Im}\, z = 0$ at $\mathrm{Re}\, z = 0$.

In our previous study,[8] we focused on a frequency window for which $\mathrm{Im}\, \varepsilon$ is small, of the order of 0.5, in which we found a 9.9% CPBG. We also found a 36.9% CPBG below the frequency window of low $\mathrm{Im}\, \varepsilon$. We considered it less relevant because we expected absorption to dominate the behavior of the fields in the frequency range where this very large CPBG occurs due to the relatively high value of $\mathrm{Im}\, \varepsilon$. Indeed, if we raise γ, thereby raising the value of $|\mathrm{Im}\, \varepsilon(\omega)|$ for all ω, we see that $|\mathrm{Im}\, z(\mathbf{k})|$ is also raised. However, Fig. 2 shows that the eigenvalues right above and below the lowest gap have an imaginary part of approximately -0.01 in units of $2\pi c/a$, which is roughly half of the typical value of -0.022 of the imaginary part of the eigenvalues located around the 9.9% gap found in the low $\mathrm{Im}\, \varepsilon$ frequency window. We compared the real part

of the complex band structure with the band structure without absorption that we calculated earlier.[8] Our previous assumption that the real part of the band structure is hardly affected by absorption turns out to be justified. If we denote by $\omega(\mathbf{k})$ the real eigenvalue without absorption, i.e., $\gamma = 0$, and by $z(\mathbf{k})$ the corresponding complex eigenvalue for $\gamma = 0.05$, then $\mathrm{Re}\, z(\mathbf{k}) - \omega(\mathbf{k})$ never exceeds 0.25% of $\omega(\mathbf{k})$ in the frequency window investigated. In other words, the real part of the band structure is hardly affected by absorption for realistic amounts of absorption. For small filling fractions ($f \approx 0.1$), this was found earlier by Kuzmiak and Maradudin.[14]

So far, all calculations presented in this paper were done for Bloch vectors on the characteristic path $\mathcal{B}_c$. In fact, virtually all published band structures, not only in the field of photonic crystals but also the conventional electronic band structures of solid-state physics, are calculated with only the characteristic path. But in the complex case, the usual arguments, justifying this procedure, break down, and, in order to see what happens, we recalculated the spectrum including $\mathbf{k}$ values outside $\mathcal{B}_c$. We found that in most cases the loops $\{z_j(\mathbf{k})|\mathbf{k} \in \mathcal{B}_c\}$ in the complex plane are filled up entirely with eigenvalues $z_j(\mathbf{k})$ for $\mathbf{k}$ outside of the characteristic path. But there are exceptions, in particular for some higher bands. Figure 3 shows a detail of the spectrum shown in Fig. 1. The eigenvalues calculated on the characteristic path are shown in black, and the ones calculated outside are shown in gray. This graph has two striking features. First, it shows the spectrum has a hole. It is small and elongated but significant, and we checked that it is not a numerical artifact. Quite recently, it was found by Gralak,[15] for a system of square rods rather than cylinders, that such structures emerge as a partial overlap of pieces of spectrum with different symmetries. Second, the black points do not enclose all eigenvalues calculated outside the characteristic path. However, it is still true that, for the real part of the band structure, the values of $\mathrm{Re}\, z(\mathbf{k})$ for $\mathbf{k} \in \mathcal{B}_c$ form a boundary for the value of $\mathrm{Re}\, z(\mathbf{k})$ for $\mathbf{k} \in \mathcal{B}$.

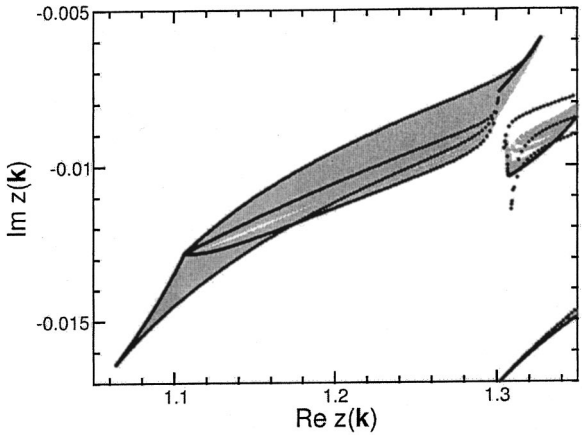

Fig. 3. Detail of Fig. 1 showing the eigenvalues in the complex plane. The black dots correspond to eigenvalues calculated for a Bloch vector on the characteristic path. The gray area represents the eigenvalues calculated for Bloch vectors that are not on the characteristic path. Note the small white area inside the gray, where no spectrum is present.

4. DISCUSSION

Using Laplace-transform techniques, we can express the electric field at time $t > 0$ in terms of the initial fields at $t = 0$ according to ($z = \omega + i\delta$, $\delta > 0$),

$$\begin{aligned}\mathbf{E}(\mathbf{x}, t) &= (2\pi)^{-1} \int \mathrm{d}\omega \exp[-izt] \langle \mathbf{x}| [z^2 \varepsilon(\mathbf{x}, z) \\ &\quad - \mathsf{H}_0]^{-1} |\mathbf{y}\rangle \{iz\mathbf{D}(\mathbf{y}, 0) - \partial_{\mathbf{y}} \times \mathbf{B}(\mathbf{y}, 0)\} \\ &= (2\pi)^{-1} \int \mathrm{d}\omega \exp[-izt] \mathsf{G}(\mathbf{x}, \mathbf{y}, z) \{iz\mathbf{D}(\mathbf{y}, 0) \\ &\quad - \partial_{\mathbf{y}} \times \mathbf{B}(\mathbf{y}, 0)\}. \end{aligned} \tag{12}$$

Although this is the case for its Bloch-decomposed components,[10] it is not obvious that $\mathsf{G}(\mathbf{x}, \mathbf{y}, z)$ itself can be continued analytically into the lower complex half-plane $\mathbb{C}_-$; the contributions to the spectrum from different $\mathbf{k}$ can in principle fill up the whole lower complex half-plane. But our computations show that the spectrum of $z^2\varepsilon(\mathbf{x}, z) - \mathsf{H}_0$ consists of bounded isolated areas in $\mathbb{C}_-$. Each of them consists of a set $\{z_j(\mathbf{k})|\mathbf{k} \in \mathcal{B}\}$. Wrapping contours around these, we then obtain contributions to $\mathbf{E}(\mathbf{x}, t)$ that decay exponentially in time except for the lowest-frequency part in the H-polarization case.

Two competing effects determine the absorption properties of a single scatterer as a function of the frequency ω of an incident field. On the one hand, $\mathrm{Im}\, \varepsilon(\omega)$ decreases with increasing frequency. Thus the attenuation of a field inside a Drude metallic cylinder becomes less with increasing frequency, tending to zero in the high-frequency limit.

On the other hand, $\mathrm{Re}\, \varepsilon(\omega)$, which has a negative value in the range considered here, determines the reflection of the fields from the metal below the plasma frequency and decreases (becomes more negative) with decreasing frequency. As a result of this effect, transmission into the absorbing material decreases with decreasing frequency, i.e., the field is more expelled from the material, and hence less absorption takes place. Thus, also in the low-frequency limit the absorption should vanish.

The competition of these two effects can be seen in the V shape formed by the eigenvalues of the H-polarized states in the complex plane, cf. Fig. 2, lower plot. For low frequencies, $\mathrm{Im}\, z(\mathbf{k})$ tends to zero with decreasing frequency ($\mathrm{Re}\, z(\mathbf{k})$), indicating that the field is increasingly expelled from the absorbing cylinders. This effect is not seen for the E polarized states, simply because there are no eigenstates with this polarization below the cut-off frequency of roughly 0.75.

For higher frequencies, roughly above $\omega a/2\pi c = 1$, $|\mathrm{Im}\, z(\mathbf{k})|$ decreases with increasing frequency, albeit not monotonically, indicating that the effect of the decrease of $\mathrm{Im}\, \varepsilon$ starts to dominate over the effect of the increase of the penetration depth due to the increase of $\mathrm{Re}\, \varepsilon$.

The highest values of the decay rate $|\mathrm{Im}\, z(\mathbf{k})|$ for the H polarization are found for frequencies around the surface-plasmon resonance frequency $\omega_{\mathrm{sp}} = \omega_p/\sqrt{2}$. As noted earlier, there are many very flat bands in this frequency region. These flat bands correspond to excitations of individual cylinder surface-plasmon resonances. These resonances are strongly localized near a cylinder surface

and have only very little overlap with the modes of neighboring cylinders. Obviously, these single-cylinder resonances do not depend on the angle of incidence, and the only effect of the lattice is their broadening into resonance bands, which look very flat compared with the Bragg bands resulting from multiple scattering. A nice discussion of this point can be found in the book by Ziman.[16] We note in passing that in the metallo-dielectric case, the effect of single-scatterer resonances is much stronger than in a purely dielectric case, which has been considered by Moroz and Tip.[17]

For the E polarization, no bands appear below $\omega a/2\pi c = 0.75$. Inside the first band, $\mathrm{Im}\, z(\mathbf{k})$ decreases with increasing frequency. This could, at least partly, be attributed to the decrease of $\mathrm{Im}\, \varepsilon$. However, the value of $|\mathrm{Im}\, z(\mathbf{k})|$ at the top of the first band is nearly 2.7 times smaller than its value at the bottom of the second band, whereas $\mathrm{Im}\, \varepsilon$ is significantly smaller in the latter case. This suggests that for complex eigenvalues with a real part at the top of a band gap (in the real part of the spectrum), the associated field modes are larger inside an absorptive scatterer than for eigenvalues at the top of the previous band. The situation is reminiscent of the Borrmann effect, previously observed in x-ray scattering.[18] The origin of this effect is that fields in the proximity of bandgap edges approach a standing wave. In the proximity of one bandgap edge, fields are mostly localized in the regions of a low dielectric constant, whereas, in the proximity of the other bandgap edge, they are mostly localized in the regions of a high dielectric constant. This sort of behavior can already be observed for a simple 1D periodic stacking of dielectric layers.[19]

For both polarizations, we find that the resonance frequencies $\mathrm{Re}\, z(\mathbf{k})$ differ less than 0.25% from the eigenfrequencies in the absorptionless case. Thus if one is only interested in the real part of the band structure of an absorptive photonic crystal, it is safe to neglect absorption.

A. Characteristic Path

It is common practice to restrict band-structure calculations to $\mathbf{k}$ values along a characteristic path. This is rigorously true for 1D Schrödinger systems, where the eigenvalues are monotonous functions of k (now a 1D parameter, ranging through an interval, its end points constituting the characteristic path). In the 3D Schrödinger case, this also gives correct results, but here the situation is different. When we no longer limit ourselves to Bloch vectors on the characteristic path connecting the points of high symmetry in the Brillouin zone, but instead consider all Bloch vectors, we find that in most cases the eigenvalues calculated for Bloch vectors on the characteristic path form a boundary of areas in the complex plane that are filled up entirely with eigenvalues calculated for Bloch vectors not on the characteristic path. However, we found several exceptions to this behavior. Figure 3 shows a few of them.

First, as noted earlier, there is a narrow, but significant, elongated hole in the spectrum roughly near $z = 1.14 - 0.012i$. We checked that this hole is not an artifact of the finiteness of the grid size of $\mathbf{k}$ points in the Brillouin zone. The hole remains no matter how much we refine the grid of $\mathbf{k}$ points. Indeed, as noted above, holes can appear by partly overlapping spectral areas with different symmetry.

Figure 3 also shows an example of a significant area, shown in gray, consisting of eigenvalues for $\mathbf{k}$ not on the characteristic path, which is not enclosed by eigenvalues calculated on the characteristic path, the points plotted in black. Both the hole in the spectrum and the presence of eigenvalues outside of the area enclosed by the eigenvalues calculated on the characteristic path imply that is no longer sufficient to calculate the spectrum only on the characteristic path.

B. Method

Our complex band structures have been calculated by combining analytic continuation in tandem with the KKR approach. This turns out to be a powerful combination that results in very fast and accurate results. The KKR method is well adapted for calculations for structures containing metals, as was already seen for calculations without absorption. Combining this method with analytic continuation in order to include absorption in the calculations hardly slows down the calculations. The latter have been performed on a regular personal computer with a single Pentium III processor at 500 Mhz. The calculations like the ones done for Figs. 1 and 2, for which the spectrum has been calculated for 504 $\mathbf{k}$ points on the characteristic path, take approximately 30 min. The speed of the calculation method becomes all the more relevant for calculating the entire spectrum, i.e., not only on the characteristic path, but for Bloch vectors in the entire Brillouin zone.

C. Related Work

Recently, Sakoda *et al.*[20] presented band-structure calculations for 2D photonic crystals with Drude metallic cylinders with parameters close to ours. Their calculations were based upon the so-called finite-difference time-domain method. According to this method, Maxwell's equations are discretized both in space and in time. The above authors numerically calculated the evolution of the discretized fields (on which Bloch boundary conditions are imposed) generated by an oscillating point dipole. From the calculated fields, both the resonance frequencies $\omega(\mathbf{k})$, corresponding to our $\mathrm{Re}\, z(\mathbf{k})$, and the decay times $\tau(\mathbf{k})$, corresponding to our $|\mathrm{Im}\, z(\mathbf{k})|^{-1}$, were extracted. Their results compare well with the results of our calculations, as far this can be judged from the graphs presented in this reference.

D. Outlook

The complex band structure we obtained gives information about the time evolution of the fields. Other interesting properties of absorptive photonic crystals include the spatial attenuation of fields propagating through such structures and decay rates of embedded excited atoms. Both are determined by the Helmholtz Green's function. Work on this subject is now in progress. Note that for atomic decay rates, only the imaginary part of the Green's function is required.[9] It replaces the usual electromagnetic density of states. The latter no longer exists, the eigenvalues now being complex.

Another matter, involving the Green's function, concerns the competition between absorption and reflection. Obviously a wave traveling through a solid piece of Drude metal, such as silver, will be completely absorbed. But if the scatterers show strong reflection (small penetration depth) in a certain frequency range, the situation can be different for a photonic crystal, even at large filling fractions.

APPENDIX A: KKR METHOD

Let Λ be a simple (Bravais) periodic lattice. According to the Bloch theorem, a propagating wave ψ in a periodic structure with the symmetry Λ is characterized by the Bloch momentum $\mathbf{k}$. The latter describes the translational properties of ψ by any lattice vector $\mathbf{r}_s \in \Lambda$,

$$\psi(\mathbf{r} + \mathbf{r}_s) = \psi(\mathbf{r})\exp(i\mathbf{k} \cdot \mathbf{r}_s). \tag{A1}$$

The Bloch property holds irrespective of the nature of a wave, i.e., it is the same for scalar and vector waves. We shall confine ourselves to the case where, outside the scatterers, the wave function ψ satisfies the scalar Helmholtz equation,

$$[\Delta + \sigma^2]\psi = 0, \tag{A2}$$

with σ being a positive constant and $\sigma^2 = \varepsilon_0\omega^2$. Let $G_{0\Lambda}(\sigma, \mathbf{k}, \mathbf{R})$ denote the free Green's function associated with the Helmholtz equation (A2) on the unit cell with Bloch boundary conditions. It can be expressed as

$$\begin{aligned} G_{0\Lambda}(\sigma, \mathbf{k}, \mathbf{R}) &= \sum_{\mathbf{r}_s \in \Lambda} G_0(\sigma, \mathbf{R} - \mathbf{r}_s)\exp(i\mathbf{k} \cdot \mathbf{r}_s) \\ &= \sum_{\mathbf{r}_s \in \Lambda} G_0(\sigma, \mathbf{R} + \mathbf{r}_s)\exp(-i\mathbf{k} \cdot \mathbf{r}_s), \end{aligned} \tag{A3}$$

where $\mathbf{R} = \mathbf{r} - \mathbf{r}'$ and G_0 denotes a free-space Green's function associated with Eq. (A2). In the 2D case considered here,

$$G_0(\sigma, \mathbf{R}) = G_0(\sigma, \mathbf{r}, \mathbf{r}') = -\frac{i}{4}H_0^+(\sigma R), \tag{A4}$$

where $R = |\mathbf{R}|$, and H_0^+ is the Hankel function of the first kind for index $m = 0$. Within the KKR method,[21,22] the band structure is determined by solving the KKR secular equation, cf. Eq. (7),

$$\det[1 - t(\sigma)g(\sigma, \mathbf{k})] = 0, \tag{A5}$$

where t is a single-scatterer scattering t matrix and g is the matrix of structure constants.[12] Both t and g are considered as matrices with matrix elements labeled by pairs of angular-momentum numbers (m, m'). In the scalar case in 2D, the matrix elements of g in the angular-momentum basis are defined as expansion coefficients of

$$\begin{aligned} &G_{0\Lambda}(\sigma, \mathbf{k}, \mathbf{R}) - G_0(\sigma, \mathbf{R}) \\ &\quad = \sum_{m,m'} g_{m,m'}(\sigma, \mathbf{k})J_m(\sigma r)\exp(im\varphi_{\mathbf{r}})J_{m'}(\sigma r') \\ &\qquad \times \exp(-im\varphi_{\mathbf{r}}), \end{aligned} \tag{A6}$$

where J_m are the regular cylindrical Bessel functions. Structure constants can be efficiently calculated by an extension of the Ewald method introduced by Ozorio de Almeida.[11]

Provided one only considers propagation of waves inside of the plane of periodicity, the wave equations for the transverse polarizations are decoupled. In this case, one can apply the scalar formalism to the Z component of either the electric field of the magnetic field, the Z axis being the coordinate axis perpendicular to the plane of periodicity.

If Λ is not a simple (Bravais) periodic lattice, i.e., there is more than one scatterer in the primitive lattice cell, the matrices t and g in Eq. (A5) become matrices with entries labeled by multi-indices $m\alpha$, where m is defined as before and α runs over all the scatterers in the primitive lattice cell.

ACKNOWLEDGMENTS

We would like to thank H. G. Muller for fruitful discussions and B. Gralak for providing the results of complex band-structure calculations for similar 2D systems.

This work is part of the research program of the Stichting voor Fundamenteel Onderzoek der Materie (Foundation for Fundamental Research on Matter) and was made possible by financial support from the Nederlandse Organisatie voor Wetenschappelijk Onderzoek (Netherlands Organization for Scientific Research).

*Present address: ESTEC/ESA Electromagnetics Division, P.O. Box 299, 2200 AG Noordwijk, The Netherlands.

REFERENCES

1. V. P. Bykov, "Spontaneous emission in a periodic structure," Sov. Phys. JETP **35**, 269–273 (1972).
2. V. P. Bykov, "Spontaneous emission from a medium with a band spectrum," Sov. J. Quantum Electron. **4**, 861–871 (1975).
3. E. Yablonovitch, "Inhibited spontaneous emission in solid-state physics and electronics," Phys. Rev. Lett. **58**, 2059–2062 (1987).
4. C. M. Soukoulis, ed., *Photonic Crystals and Localization in the 21st Century*, NATO ASI Ser. Ser. C **563** (2001).
5. A. Moroz, "Three-dimensional complete photonic-band-gap structures in the visible," Phys. Rev. Lett. **83**, 5274–5277 (1999).
6. A. Moroz, "Photonic crystals of coated metallic spheres," Europhys. Lett. **50**, 466–472 (2000).
7. A. Moroz, "Metallo-dielectric diamond and zinc-blende photonic crystals," Phys. Rev. B **66**, 115109 (2002).
8. H. van der Lem and A. Moroz, "Towards two-dimensional complete photonic bandgap structures below infrared wavelengths," J. Opt. A: Pure Appl. Opt. **2**, 395–399 (2000).
9. A. Tip, "Linear absorptive dielectrics," Phys. Rev. A **57**, 4818–4841 (1998).
10. A. Tip, A. Moroz, and J. M. Combes, "Band structure for absorptive photonic crystals," J. Phys. A **33**, 6223–6252 (2000).
11. A. M. Ozorio de Almeida, "Real-space methods for interpreting electron micrographs in cross-grating orientations. I. exact wave formulation," Acta Crystallogr. Sect. A **31**, 435–442 (1975).

12. J. S. Faulkner, "Multiple-scattering calculations in two dimensions," Phys. Rev. B **38**, 1686–1694 (1988).
13. A. Moroz, "Density-of-states calculations and multiple-scattering theory for photons," Phys. Rev. B **51**, 2068–2081 (1995).
14. V. Kuzmiak and A. A. Maradudin, "Photonic band structures of one- and two-dimensional periodic systems with metallic components in the presence of dissipation," Phys. Rev. B **55**, 7427–7444 (1997).
15. B. Gralak, FOM-Instituut voor Atoom en Molecuulfysica, Amsterdam, The Netherlands (personal communication, 2002).
16. J. Ziman, "The T matrix, the K matrix, d bands and l-dependent pseudo-potentials in the theory of metals," Proc. Phys. Soc. London **86**, 337–353 (1965).
17. A. Moroz and A. Tip, "Resonance-induced effects in photonic crystals," J. Phys. Condens. Matter **11**, 2503–2512 (1999).
18. W. H. Zachariasen, *Theory of X-ray Diffraction in Crystals* (Dover, New York, 1945).
19. P. S. J. Russel, "Photonic band gaps," Phys. World **37**, 37–41 (1992).
20. K. Sakoda, N. Kawai, T. Ito, A. Chutinan, S. Noda, T. Mitsuyu, and K. Hirao, "Photonic bands of metallic systems. I. Principle of calculation and accuracy," Phys. Rev. B **64**, 045116 (2001).
21. J. Korringa, "On the calculation of the energy of a Bloch wave in a metal," Physica (Utrecht) **13**, 392–400 (1947).
22. W. Kohn and N. Rostoker, "Solution of the Schrödinger equation in periodic lattices with an application to metallic lithium," Phys. Rev. **94**, 1111–1120 (1954).